JOURNAL OF BACTERIOLOGY, Sept 1974, p. 1019-1038
Vol. 119, No. 3

Superficial Macromolecular Arrays on the Cell Wall of *Spirillum putridiconchylium*

T. J. BEVERIDGE AND R. G. E. MURRAY

Department of Bacteriology and Immunology, University of Western Ontario, London, Ontario, Canada

Received for publication 30 May 1974

Electron microscopy of the cell envelope of *Spirillum putridiconchylium*, using negatively stained, thin-sectioned, and replicated freeze-etched preparations, showed two superficial wall layers forming a complex macromolecular pattern on the external surface. The outer structured layer was a linear array of particles overlying an inner tetragonal array of larger subunits. They were associated in a very regular fashion, and the complex was bonded to the outer, pitted surface of the lipopolysaccharide tripartite layer of the cell wall. The relationship of the components of the two structured layers was resolved with the aid of optical diffraction, combined with image filtering and reconstruction and linear and rotary integration techniques. The outer structural layer consisted of spherical 1.5-nm units set in double lines determined by the size and arrangement of 6- by 3-nm inner structural layer subunits, which bore one outer structural layer unit on each outer corner. The total effect of this arrangement was a double-ridged linear structure that was evident in surface replicas and negatively stained fragments of the whole wall. The packing of these units was not square but skewed by 2° off the perpendicular so that the "unit array" described by optical diffraction and linear integration appeared to be a deformed tetragon. The verity of the model was checked by using a photographically reduced image to produce an optical diffraction pattern for comparison with that of the actual layers. The correspondence was nearly perfect.

Regular macromolecular surface arrays (RS) have been demonstrated on the cell walls of both gram-positive and gram-negative bacteria (13). Among gram-positive genera, RS layers have been identified on species of *Bacillus* (11, 16, 21, 31) and *Clostridium* (13). A larger number of gram-negative genera show RS layers and diversity of structural arrangements, e.g., species of *Spirillum* (5, 6, 30), *Rhodospirillum* (13), *Azotobacter* (13), *Cardiobacterium* (32), *Selenomonas* (13), *Ectothiorhodospira* (13), *Acinetobacter* (36, 39), and *Lampropedia* (8). These are usually single layers of complex protein subunits (7, 18, 38, 40) arranged in one of two patterns, hexagonal or tetragonal (5, 13). In the case of the gram-positive cell, these regular arrays appear to position themselves along the outer surface of a homomorphic cell wall containing peptidoglycan, teichoic acid, and other components (18, 31), whereas those of the gram-negative cell lie external and adjacent to the outer lipopolysaccharide (LPS) membrane (6, 7, 30, 32, 36, 40). There are a few examples of the superimposition of these superficial arrays of macromolecules, such as the juxtaposition of hexagonal and tetragonal patterns on the walls of *Nitrosococcus* (*Nitrosocystis*) *oceanus* (41) and in the spore coats of some *Bacillus* species (16). These patterned layers are superficial cell wall constituents and are associated in some formal way with underlying components of the wall; in the case of *Spirillum serpens*, there is evidence of bonding to the immediately adjacent LPS layer (6, 7), but in most cases the nature of the association is unknown. They appear to be distinct from the much less regular arrays of the lipoprotein component of the walls of the *Enterobacteriaceae*, which lie between the mucopeptide and LPS layers of the cell wall (2, 3, 4).

The techniques of linear and rotary integration (27, 28) and optical diffraction (19, 20, 37) have given the morphologist powerful tools to resolve form and arrangements in these RS layers, which are of such paracrystalline regularity that these techniques can be applied.

Spirillum putridiconcylium provided us with an example of a very complex arrangement requiring high resolution. At first sight it presented a linear superficial array, but, on closer examination, was found to overlie and be integrated with a layer of a different arrangement

and spacing. This paper describes the structures and the interpretation of their interrelations.

MATERIALS AND METHODS

Organisms. *S. putridiconchylium* (ATCC 15279) was obtained from N. R. Krieg (Department of Biology, Virginia Polytechnic Institute, Blacksburg, Va.); strain #21 was derived from it after nitrosoguanidine treatment (1) and selected as a colony variant which exhibited a deficiency in the structure of the outer layer of the cell wall.

Cultivation. Both organisms were maintained at 30 C in peptone-succinic acid-salts-yeast extract semisolid medium consisting of 0.75% peptone (Difco), 0.1% succinic acid (Fisher Scientific), 0.1% yeast extract (Difco), 0.1% $MgSO_4 \cdot 7H_2O$, 0.1% $(NH_4)_2SO_4$, 0.0002% $FeCl_3 \cdot 6H_2O$, 0.0002% $MnSO_4 \cdot H_2O$, 0.111% $CaCl_2$ (all salts were reagent grade, McArthur Chemical Co., Montreal, Que.), and 0.15% agar (Difco). This medium was adjusted to pH 7.0 with 1 N KOH. For electron microscopic studies the cells were grown in 50 ml of peptone-succinic acid-salts-yeast extract broth at 30 C on a rotary shaker until either mid or late logarithmic growth was established (mean generation time = 51.2 min). Calcium (1 mM $CaCl_2$) in the medium was essential to maintain the integrity of the RS components.

Preparations for electron microscopy. (i) Negative staining technique. Samples of the cell suspension or wall fragments were mixed either 1:2 with 1% ammonium molybdate, 1:1 with 2% uranyl oxalate, or 1:2 with 0.1 M sodium zirconyl glycolate (6). All negative stains contained 1 mM $CaCl_2$. Each stain was filtered through a Swinnex-13 filter holder containing a 0.45-μm membrane filter (Millipore Corp.) immediately before use. The stain-cell suspensions were well mixed and spread by breaking a thin film in a 3.5-mm loop over the surface of a 3-mm carbon-Formvar-coated 400-mesh copper grid.

(ii) Fixing, embedding, and sectioning technique. Prefixation was attained by adding 0.1 ml of 10% acrolein (Eastman Kodak Co., Rochester, N.Y.) in 0.2 M cacodylic acid buffer, pH 7.2, and 0.1 ml of 8% glutaraldehyde (Polysciences Inc., Warrington, Pa.) in distilled water to 10 ml of broth culture and mixing and incubating at 23 C for 15 min. The suspension was then centrifuged into a pellet and resuspended for fixation in 0.1 M cacodylic acid buffer (pH 7.2) containing 1 mM $CaCl_2$ (CAC buffer), 5% acrolein, and 4% glutaraldehyde for 1 h at 23 C. The cells were then washed five times with 10 ml of CAC buffer, enrobed in 2% Noble agar (Difco) in CAC buffer, cut into 1-mm blocks, and postfixed with 1% OsO_4 in CAC buffer for 2 h at 23 C. After postfixation the material was washed twice with 10 ml of CAC buffer for 30 min each and stained for 2 h in either 2% uranyl acetate or 1% uranyl magnesium acetate (K & K Laboratories Inc., Plainview, N.Y.). After staining, the agar blocks were washed twice with 1 mM $CaCl_2$ for 15 min.

A fixation procedure utilizing ruthenium red (British Drug Houses Chem. Ltd., Poole, England) was also used. In this case 500 μg of ruthenium red per ml was incorporated into both the fixative and postfixative solutions in CAC buffer. In a few instances, 1% alcian blue 8GX (Taab Lab., Reading, England) was substituted for ruthenium red in the fixative schedule.

Four embedding media were used with various handling techniques: Vestopal W (Martin Jaeger, Vesenaz, Geneva, Switzerland), Epon (Ladd Research Industries, Burlington, Vt.), hydroxypropyl methacrylate (HPMA) (Polysciences Inc., Warrington, Pa.), and Durcupan (Fluka AG, Buchs SG, Switzerland). For Vestopal embedding, the agar blocks were first dehydrated in increasing concentrations of acetone containing 1 mM $CaCl_2$, infiltrated with monomer, and cured (15, 34) under vacuum at 60 C for 56 h. For Epon 812 embedding, the blocks were dehydrated through increasing ethanol concentrations and then through increasing propylene oxide concentrations (15, 23). Curing occurred under vacuum at 60 C for 56 h. For HPMA embedding, the agar blocks were dehydrated by means of two changes of 85% HPMA followed by two changes of 97% HPMA (each containing 1 mM $CaCl_2$). Two changes (30 min each) of prepolymerized solutions (95% HPMA containing 0.1% azobis-iso-butyronitrile and heated to 120 C for 5 to 10 min) preceded the final embedding. They were cured at 4 C under ultraviolet light (315 nm) for 56 h (15, 22). For Durcupan embedding, the agar blocks were put in a 70% aqueous solution of component A (the water-soluble aliphatic polyepoxide), containing 1 mM $CaCl_2$, for 30 min, followed by a 90% component A-1 mM $CaCl_2$ solution for 30 min and then by two changes of 100% A for 1 h each. The blocks were then put into a complete Durcupan embedding mixture and left for 1 h at 23 C and then changed once and refrigerated at 4 C overnight. The blocks were then brought to 23 C, embedded in fresh complete Durcupan, and cured at 40 C for 56 h (15).

All embeddings were cut on a Reichert model OMU2 ultramicrotome with glass knives, and sections were collected on carbon-Formvar-coated 200-mesh copper grids. The sections were stained with either 1% uranyl acetate and lead citrate (33) or with 500 μg of ruthenium red per ml.

For silver methenamine stains, the sections were treated according to the procedure of de Martino and Zamboni (10).

(iii) Freeze-etching technique. Samples for freeze-etching were processed according to Buckmire and Murray (6). Samples were stored in liquid nitrogen for no longer than 48 h. Etching times varied between 30 to 90 s. Cryogens were not utilized, since both surface structure damage and inappropriate cleavage resulted. The apparatus used was a Balzers model BA510M (FL-9496 Balzers, Fürstentum Liechtenstein).

Electron microscopy. A Philips EM-300 electron microscope operating at 60 kV was used throughout. Micrographs were taken on Kodak fine-grain positive film. Negatively stained catalase crystals (Worthington Biochemicals Corp., Freehold, N.J.) were used as a calibration standard (9).

Linear integration. Linear integration was per-

formed according to Markham et al. (28). Positive transparencies (10 by 8 inch [ca. 25.4 by 20.3 cm]) of both uranyl oxalate- and ammonium molybdate-stained structures were integrated. Magnifications of approximately 300,000 to 600,000× were commonly used. Results were recorded on Polaroid 4 by 5 inch (ca. 10.1 by 12.7 cm) type 55 P/N film.

Rotary integration. A stroboscopic method of rotary integration was used (17, 27). In general, a disk speed of 400 rpm was used with stroboscopic flash frequencies of 400 to 2,500 cycles/min. The images were recorded on Kodak Panatomic X 35-mm film developed in Kodak D19 for 4 min to increase contrast.

Optical diffraction. Optical diffraction (19, 20, 37) was performed upon selected parts of micrographs enlarged upon a 3¼- by 4-inch (ca. 8.5- by 10.2-cm) sheet of electron image film (Ester Thick Base, Canadian Kodak Co. Ltd., Canada) or a 5- by 4-inch (ca. 12.7- by 10.2-cm) sheet of Cronar Ortho A litho film (E. I. duPont de Nemours & Co., Inc., Wilmington, Del.) using a Polaron optical diffractometer (Polaron Instruments Ltd., London, England) with a Spectra Physics, model 132, helium-neon laser as a light source. Optical diffraction patterns were recorded on Kodak Panatomic X 35-mm film.

A mask to allow optical reconstruction using selected diffraction points was obtained by exposing a 4- by 4-cm square of Kodak Panalure F photographic paper to the diffraction image. The developed, fixed, and dried print of the diffraction transform was then taped to a 4- by 4-cm square of blackened (light exposed and developed) film. The diffraction spots on the print were then drilled through the photographic film; the size of the drill bit was chosen in proportion to the diameter of the spot. The drilled photographic film was then mounted on a prepunched, blackened, 4 by 4 cm, cardboard square, the punched holes being of slightly larger diameter but exactly positioned with respect to the holes in the photographic film.

We found that this method of mask production resulted in an exact reproduction of the optical diffraction pattern and gave a smooth, clean mask hole and minimal aberrations without allowing stray laser emissions through. The optical reconstructions were recorded on Kodak Panatomic X 35-mm film.

Model system. The model used for optical diffraction was drawn with India ink on white paper at a scale of 1 cm = 1 nm. This was photographed with Kodak Ortho high contrast 35-mm film. The image was then reduced, using a Durst S45 enlarger as a camera, to a size such that the spacing was close to that of the electron microscope transparencies. This image was then used for confirmatory optical diffraction.

RESULTS

Negatively stained preparations. Negatively stained cells of *S. putridiconchylium* demonstrated regular arrays of macromolecules overlying the outer membrane surface. Trials with a variety of metal salts showed that ammonium molybdate and uranyl oxalate were the negative strains of choice for demonstrating detail in these RS layers, (i.e., both had small particle size, good penetration between subunit arrays, and no discernible deleterious effect on subunit integrity). The structure was poorly preserved, unless calcium salts were included in both the growth medium and the negative stain. As a result, 1 mM $CaCl_2$ was routinely added throughout this study.

Observations of log-phase cells in ammonium molybdate (pH 7.2) demonstrated linear arrays of small subunits, oriented in parallel to the cell axis, which completely encompassed the cell surface (Fig. 1, 2). Accurate measurement and interpretation of these units on the intact cell was difficult because of their small size, superimposition of structures, and distortion due to drying. Useful information was obtained from the cell margins (Fig. 2, 25, 27) where the layers were flattened and folded over. These micrographs showed 3- to 5-nm units of 7-nm periodicity separated from the wall profile by approximately 8 nm. It was clearly a superficial structured layer. Phosphotungstic acid likewise effectively demonstrated the structure, but the larger particle size of this stain was undesirable for resolution and measurement.

Staining procedures using aqueous solutions of uranyl acetate or uranyl magnesium acetate (pH ca. 4.5) effectively disrupted the superficial structure and left a loosely attached and amorphous material. A series of preparations using 0.1 M sodium zirconyl glycollate, which is stable over a wide pH range, adjusted to pH 7.0 → 4.0, demonstrated the dissociation of RS at pH 4.5 in the presence of 1 mM $CaCl_2$. Uranyl acetate containing 0.05 M oxalic acid can be adjusted to pH neutrality with ammonium hydroxide (14, 29) without discernible loss of stability. This stain revealed a surface structure and periodicity comparable to that seen with ammonium molybdate, indicating that it is the low pH and not the uranyl ion which exerts this deleterious effect.

A small proportion of stationary-phase cells showed areas of wall devoid of structure (Fig. 3), and corresponding fragments of RS were recovered from the medium by centrifugation. The fragments were appropriate for resolution of the subunit arrangement using both ammonium molybdate (Fig. 4A) and uranyl oxalate (Fig. 4B). Ammonium molybdate was the more effective and showed that small subunits of approximately 3-nm periodicity contributed the linear elements to the array. The pairs of delicate lines formed by these elements were about 3 nm apart, and each of the pairs was

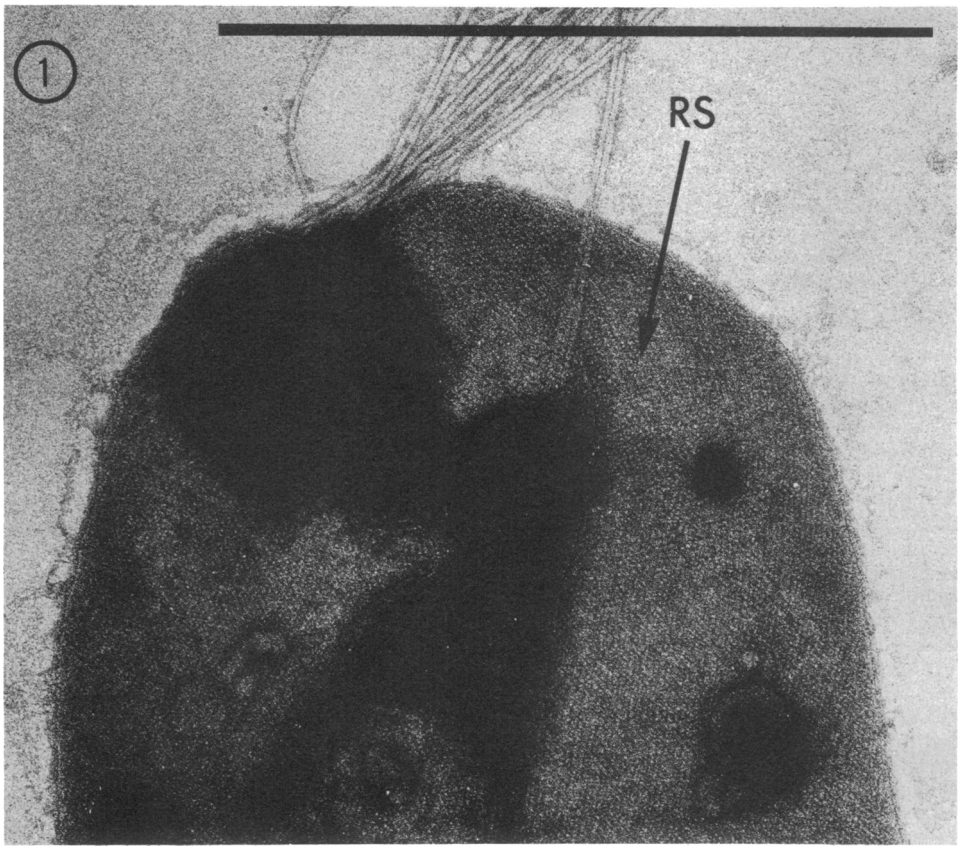

FIG. 1. *Ammonium molybdate-stained cell. RS seen as striations running along the cell surface. Bar = 1 μm. (All figures except 12 and 13 are of strain ATCC 15279).*

separated by a stain-filled space 4 to 5 nm wide. Rotation of Fig. 4A at eye level exposes two major series of subunit alignments at 70° and 106° and one intermediate alignment at 88° with respect to the primary longitudinal (linear) alignment. These alignments may also be seen, but less clearly, in uranyl oxalate preparations (Fig. 4B). Similar fragments were retrieved from the medium of late stationary-phase cultures. A small number showed a tetragonal arrangement (Fig. 5) which was entirely unexpected and remarkably different from the linear structure.

Replicated freeze-etched preparations. Cells frozen without the use of cryogens exhibited a preference for cleavage in the cell wall, whereas those frozen with the aid of glycerol exhibited a preference for cleavage at or in the plasma membrane. Cleavages along a plane exposing the RS usually revealed its exterior convex surface (Fig. 6).

The individual units of the linear array were not resolved by this technique, although the linear arrangement was verified; however, the impression was given of a series of depressions along the length of each linear order at 7-nm intervals, which was approximately twice the periodicity of the units stained by ammonium molybdate.

Cleavages between the superficial structure layers and the surface of the LPS membrane were common (Fig. 6, 7A). This surface was covered with 4-nm pits having an approximate center-to-center spacing of 7 nm. Optical diffraction of selected areas of this layer suggested that these pits are arranged hexagonally (Fig. 7B), which was a greater order of regularity than observed in the same situation for *S. serpens*. Since only selected areas of the total exposed LPS surface exhibited this hexagonal character, it is difficult to make a definitive statement as to the arrangement of these pits.

Mutants with defective superficial cell wall layers were obtained with nitrosoguanidine treatment (1). One of these (mutant #21) possessed as disrupting superficial structure (Fig.

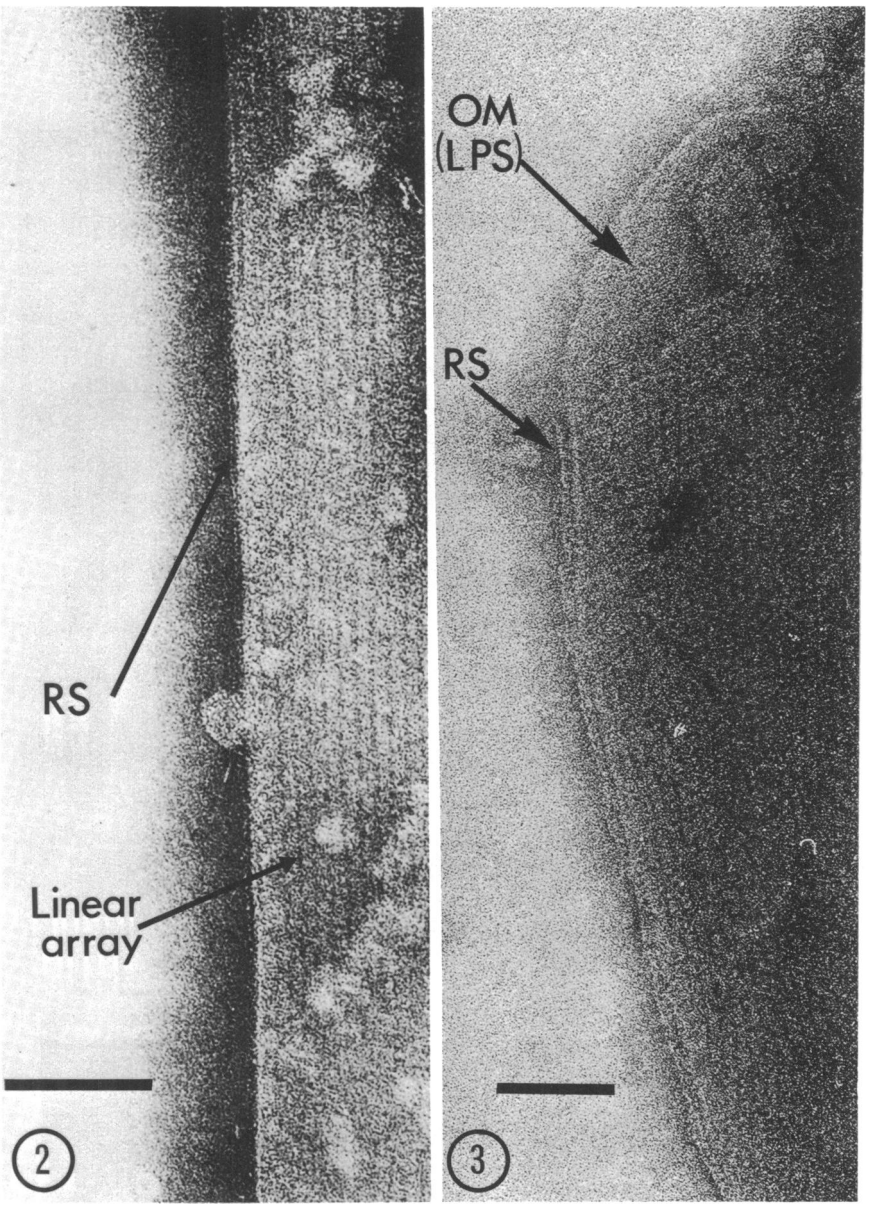

FIG. 2. *Ammonium molybdate-stained cell showing the linear array running parallel to the cell axis. The RS profile may be seen at the cell edge. Bar = 0.1 μm.*

FIG. 3. *Ammonium molybdate-stained, stationary-phase cell demonstrating the fragmentation of RS from the outer membrane (OM). Bar = 0.1 μm.*

13). Freeze-etching of this strain revealed a linear array identical to the parent strain and an underlying tetragonally packed arrangement of subunits (Fig. 12) similar in size, shape, and periodicity to those seen in Fig. 5. The latter was often overlayed with small fibrils (arrow, Fig. 12), presumably remnants of the disrupting outer layer. This suggested two morphologically distinct macromolecular layers, namely, the possibility of an outer structured layer (OSL) of linearly arranged particles which covered an inner structured layer (ISL) of tetragonally packed subunits. Cleavages which ran between these two RS layers were not found in freeze-etched preparations of the parent strain.

Thin sections. Visualization of the two RS

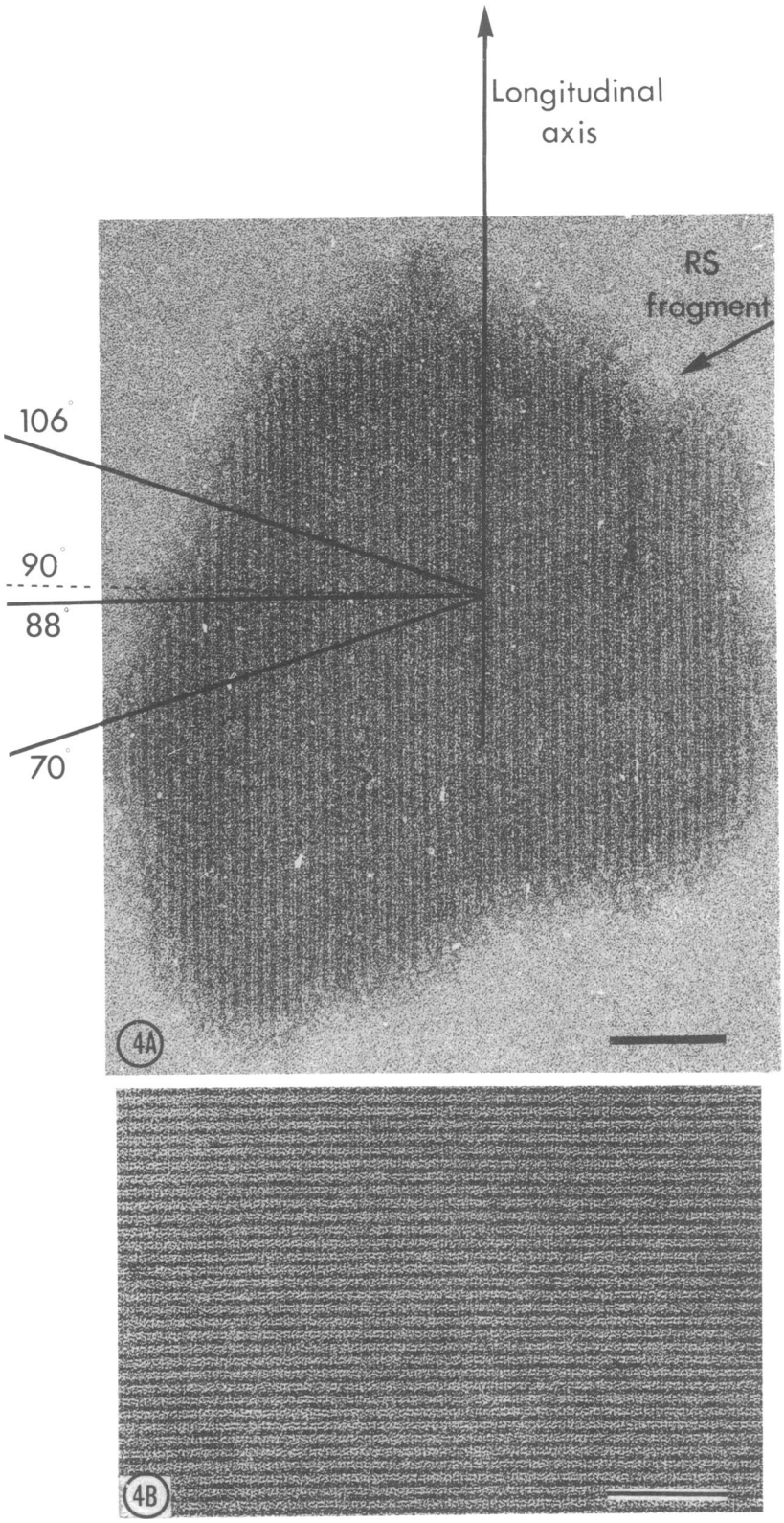

FIG. 4. *(A) Ammonium molybdate-stained intact RS fragment on which the subunit alignment angles (70°, 88°, and 106°) are shown. The longitudinal axis runs along the direction of the linear array. Bar = 0.1 μm. (B) Uranyl oxalate-stained, intact RS fragment. Bar = 0.1 μm.*

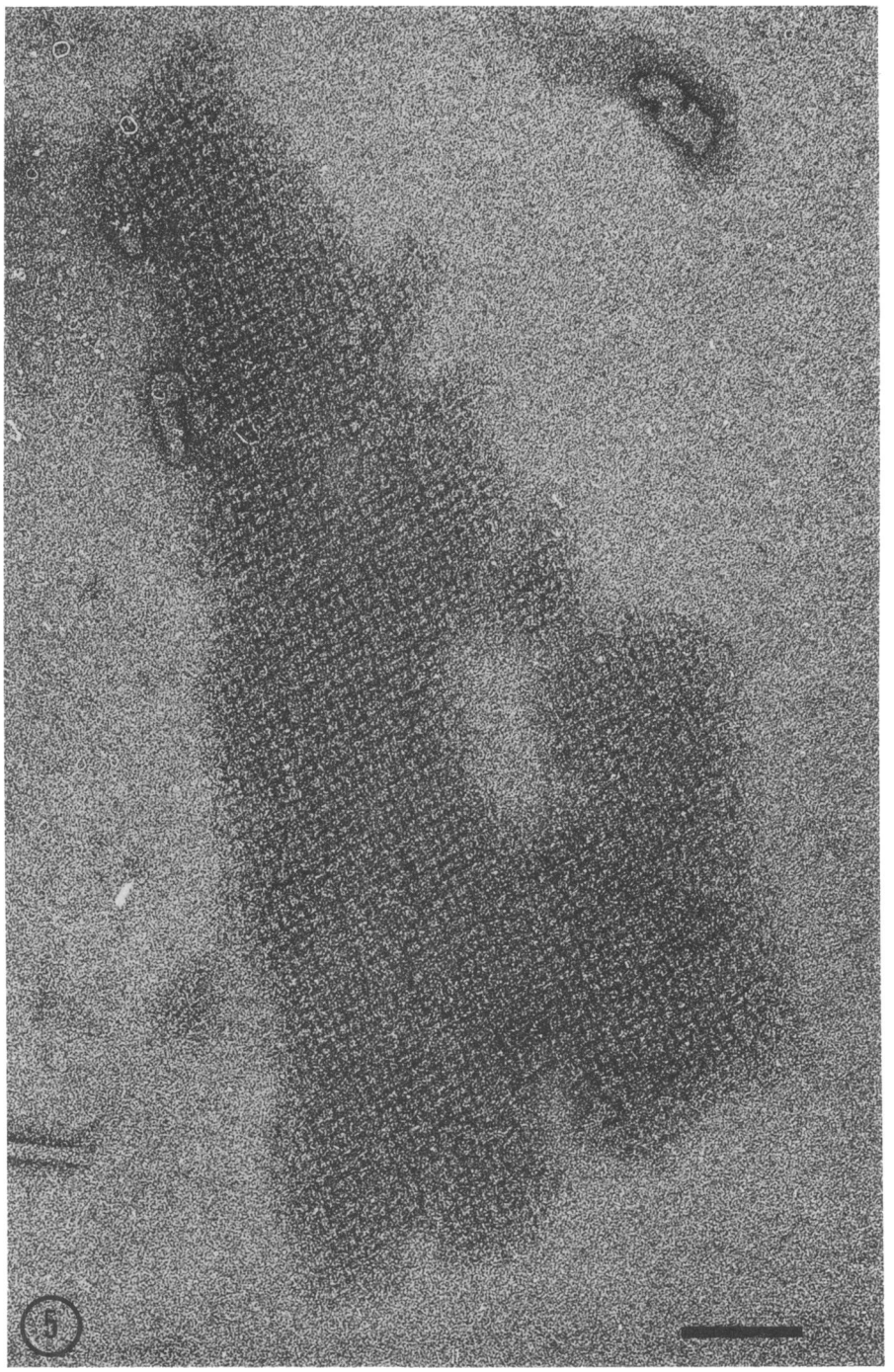

FIG. 5. *Ammonium molybdate-stained, partially intact RS fragment on which the ISL is clearly seen. Bar = 0.1 μm.*

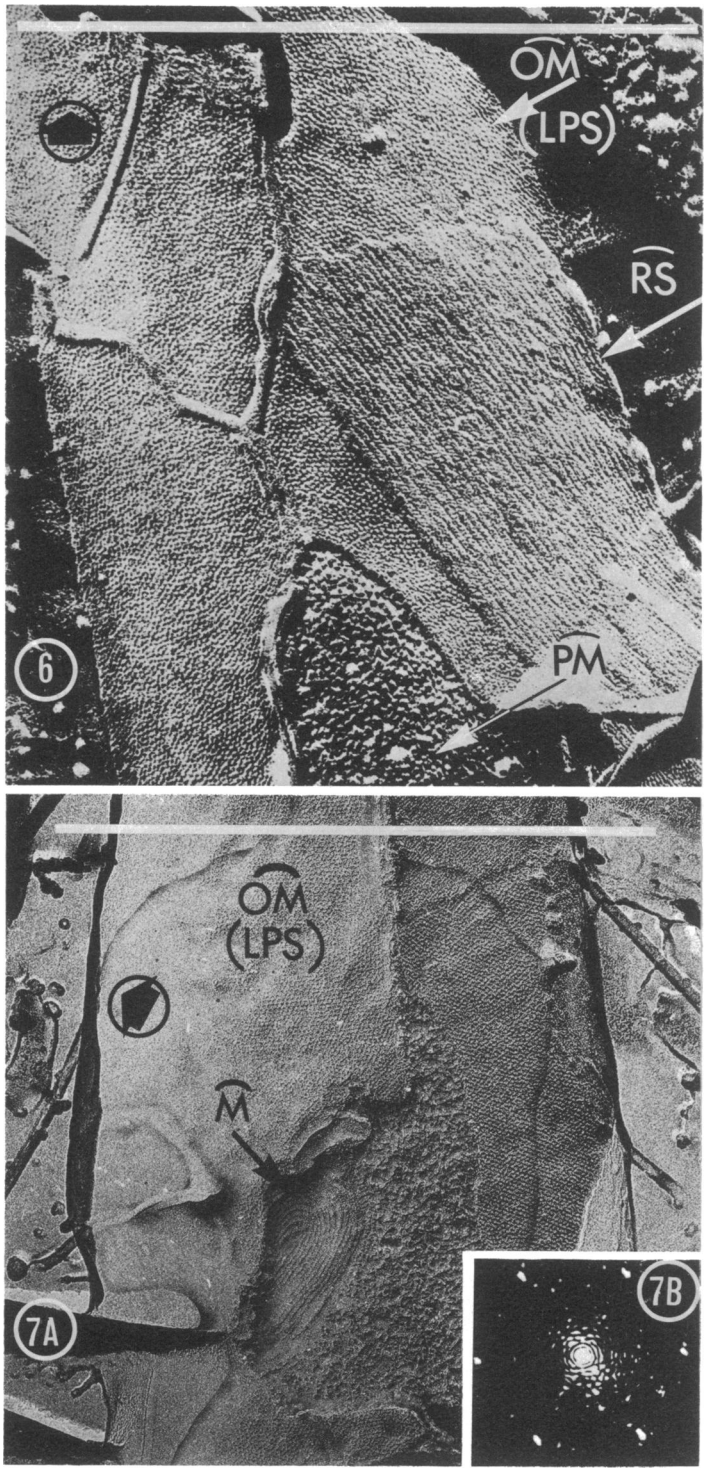

FIG. 6. *Nonreversed, freeze-etched replica showing the linearity of the RS and the underlying pitted surface of the OM. The hydrophobic plasma membrane (PM) is studded by many particles. The large arrow denotes the shadow direction. Bar = 1 μm.*

FIG. 7. *(A) Nonreversed, freeze-etched replica demonstrating the pitted surface of the OM. A mesosome (M) can be seen in the underlying cytoplasm. The large arrow denotes the shadow direction. Bar = 1 μm. (B) Optical transform, derived from the OM surface of Fig. 7A, which demonstrates the hexagonal array of pits.*

layers in thin section proved extremely difficult by normal preparatory techniques. Walls of cells embedded in either Epon 812 or Vestopal W contained no evidence of these structures and presented a "typical" gram-negative cell wall in cross section (Fig. 8). Negatively stained preparations of cells during the fixation and dehydration steps showed that the RS was susceptible to even small concentrations of the organic solvents used for dehydration, despite the maintenance of the suitable Ca^{2+} concentration throughout the series. As a result, two water-soluble embedding media were tried, Durcupan and HPMA, even though the cells were distorted. Again, 1 mM $CaCl_2$ was required throughout the fixation, block staining, and initial aliphatic polyepoxide infiltration procedures. The addition of ruthenium red, but not alcian blue, to the aldehyde fixation and OsO_4 postfixation appeared to encourage the retention of the structure (Fig. 10, 11). Cross section of the RS layers suggested two RS layers and revealed 8- by 3- to 6-nm ISL subunits immediately overlying the LPS-tripartite membrane. (Fig. 10, 11). One and one-half nm OSL units rested on the upper corners of most ISL subunits (Fig. 9–11). Some sections suggested that the ISL subunit narrowed at its middle (see arrows, Fig. 11), whereas others suggested a simple "brick" shape (Fig. 10).

Linear integration of negatively stained RS fragments. Further resolution of the component structures of ammonium molybdate-stained RS fragments required reduction of "noise" and more favorable contrast, which was obtained by mechanical image averaging (linear integration) using multiple exposures while moving the image through defined repeat intervals to identify periodicities along axes of symmetry. A repeating structure at 7- to 8-nm intervals was identified in the 4- to 5-nm space between the pairs of tracks (Fig. 14). These 3- by 5-nm subunits appeared to lie below the double track subunits of the OSL, since they were partially hidden by the stain and only the reinforcement of their image by this technique suggested their existence. Concentrating on these newly exposed subunits and neglecting the overlying double track, it was evident that the tetragon formed by nine subunits (Fig. 14) was the minimal array needed to describe the three axes of alignment (cf. optical diffraction reconstruction, Fig. 17). The axes of the tetragon were slightly skewed in a clockwise direction so that the three alignment angles, other than the longitudinal (linear aligned) axis, occured at 106°, 88°, and 70°, respectively. Linear integration at suitable periodicities along these axes also increased the contrast of these subunits and supported the view that these alignment angles were real (Fig. 15, integration performed 70° off the longitudinal axis). It was noted that the dimensions of these subunits were of the same order as for the tetragonal array in late-stationary wall fragments (Fig. 5), but the spacing and alignments were different.

It was evident that the underlying units (ISL) bore a regular relationship to the units comprising the linear tracks (OSL) forming a bridge between a lateral pair of OSL units of adjacent tracks (see diagrams, Fig. 15). In essence, it appeared that the best interpretation of the images placed each of the OSL units on the outer corners of the larger and somewhat rectangular ISL units. The shape of the ISL units could not be further resolved with any degree of accuracy and, for simplicity, have been represented as blocks proportional to the space they occupy. The "unit array" of the ISL (see Fig. 14) produced a corresponding skew in the OSL alignment (Fig. 15), suggesting an intimate relationship between OSL and ISL units. This is represented diagrammatically in Fig. 20 and, given the correct proportions for the ISL unit, reproduced the angles (70°, 88°, and 106°) of reinforcement that were identified visually in Fig. 14 and 15.

Optical diffraction and reconstruction of image of RS fragments. Optical diffraction was performed on selected areas of micrographs of negatively stained intact fragments (Fig. 4A, 4B) to resolve the OSL-ISL alignment further. Ammonium molybdate- and uranyl oxalate-contrasted fragments gave similar diffraction patterns (Fig. 16). Catalase crystals, stained in a similar manner, were used to calibrate the diffractometer (17) and to insure accurate measurement of the OSL-ISL subunit periodicities. The skewed tetragonal "unit array" of the ISL, found by linear integration, was described by spots indexed 200, 110, 020, $\bar{1}10$, $\bar{2}00$, $\bar{1}\bar{1}0$, $0\bar{2}0$, and $1\bar{1}0$. Indexes 610, 410, $\bar{3}20$, $\bar{4}10$, $\bar{6}10$, $\bar{6}\bar{1}0$, $4\bar{1}0$, $3\bar{2}0$, $4\bar{1}0$, and $6\bar{1}0$ described the alignment of the OSL pair resting on longitudinally adjacent ISL subunits, whereas indexes 500, 300, $\bar{3}00$, and $\bar{5}00$ described the linearity of the RS. Analysis of these transforms suggested that the ISL consisted of 6- by 3-nm subunits with a 1.5-nm OSL subunit residing on each corner. Taking series 020, 000, $0\bar{2}0$ as the base line of the transform we found the remaining spots skewed 2° to 4° off the perpendicular in an anticlockwise direction. Small angular discrepancies (ca. 4°) were also seen between the intersections of series 110, 000, $\bar{1}10$ and series $\bar{1}10$, 000, $1\bar{1}0$ with

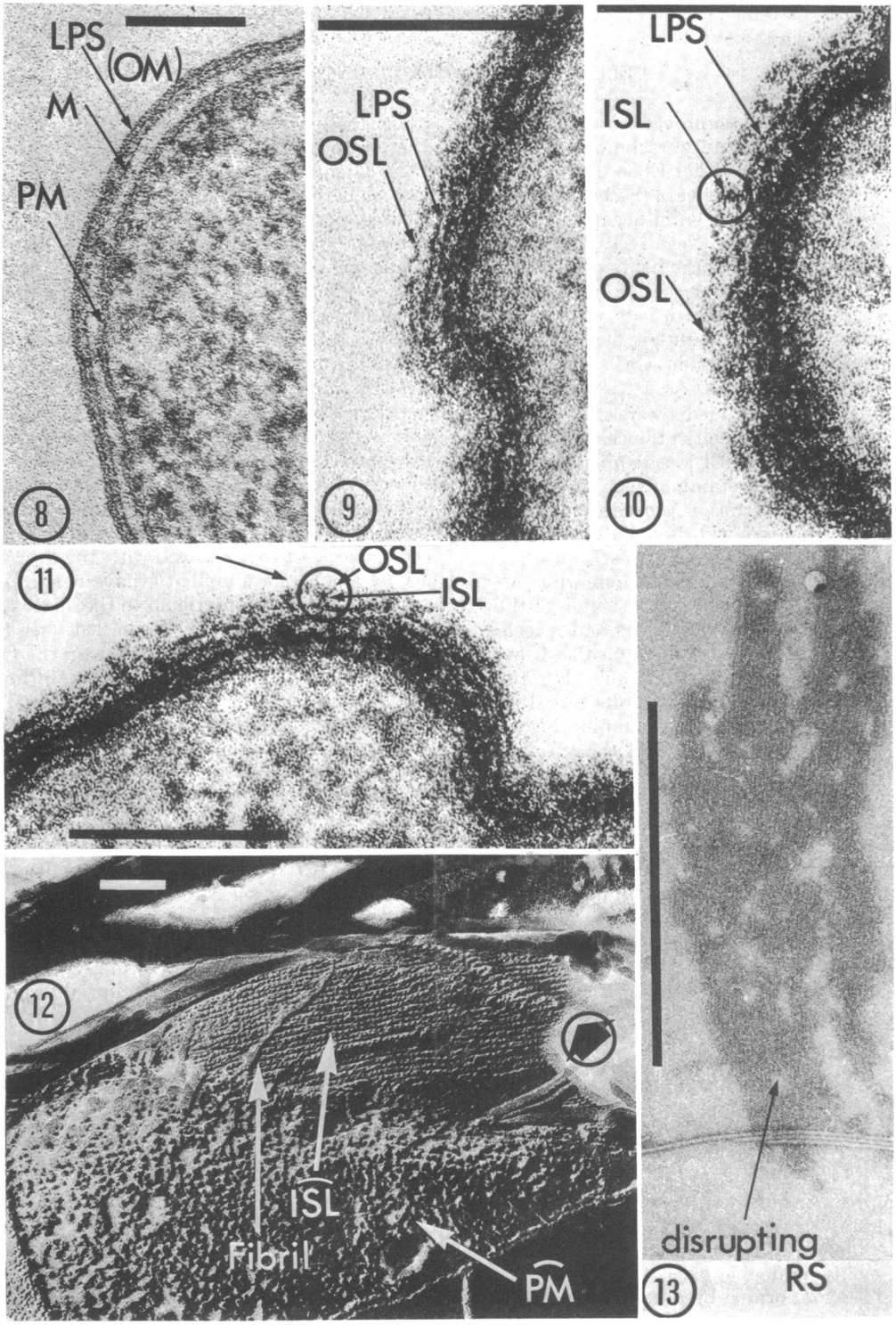

FIG. 8. *Thin section of the cell envelope of an ethanol-dehydrated and Epon 812-embedded cell. Although the plasma membrane (PM), mucopeptide (M), and LPS can clearly be seen, the RS is conspicuously absent. Bar = 0.1 μm.*

FIG. 9. *Thin section of the cell envelope of a water-miscible, Durcupan-embedded cell. Although the cell envelope is stain-clogged, a RS (OSL) can be seen overlying the LPS. Bar = 0.1 μm.*

FIG. 10. *Thin section of the cell envelope of a ruthenium red-treated and Durcupan-embedded cell. Both the OSL and the ISL can be seen overlying the LPS; in this instance, the ISL profile is rectangular in shape (see circled unit). Bar = 0.1 μm.*

FIG. 11. *Thin section of the cell envelope of a cell treated as in Fig. 10; in this instance, the ISL profile is narrowed at the waist (see circled unit). Bar = 0.1 μm.*

FIG. 12. *Nonreversed, freeze-etched replica of OSL defective mutant (strain #21) demonstrating the ISL surface. In this preparation the tetragonal shape of the ISL units can be seen, whereas in Fig. 6 they are partially*

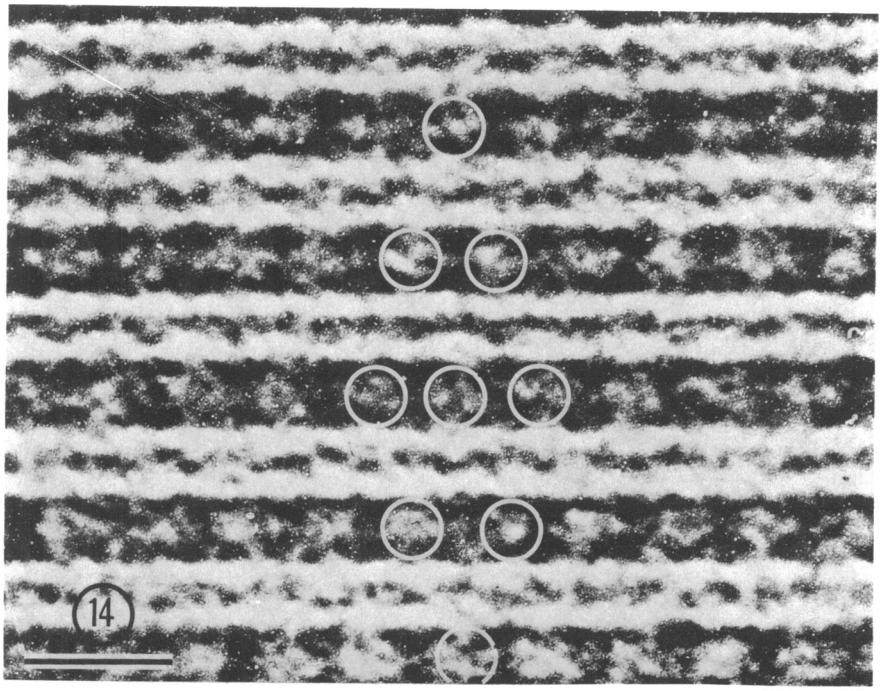

integration direction

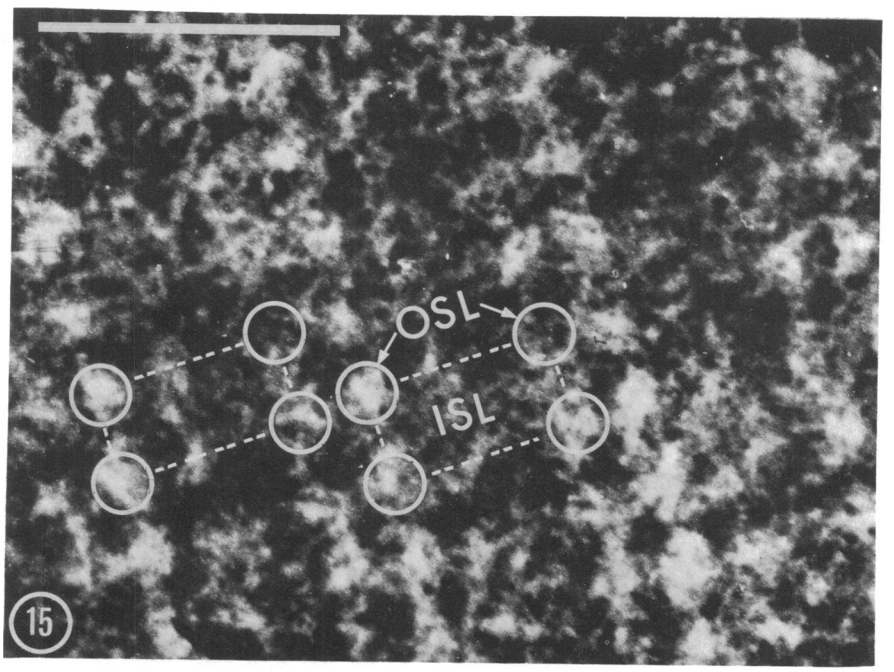

FIG. 14. *Multiple exposure after linear integration along the longitudinal axis of an ammonium molybdate-stained, intact RS fragment. This photograph has been slightly underexposed to demonstrate the skewed tetragonal array of the ISL. Number of exposures = 18; stroboscopic frequency = 7 nm; bar = 10 nm.*

FIG. 15. *Multiple exposure after linear integration of an ammonium molybdate-stained, intact RS fragment along the 70° alignment axis, demonstrating the lateral alignment of OSL and ISL units. Number of exposures = 12; stroboscopic frequency = 9.4 nm; bar = 10 nm.*

---

masked by the linearity of the small OSL units. The fibril overlying the ISL is supected to be the disrupted OSL. The large arrow denotes shadow direction. Bar = 0.1 μm.

FIG. 13. *Ammonium molybdate-stained RS fragment from mutant strain #21 showing the friable nature of the structure (probably both OSL and ISL). Bar = 1 μm.*

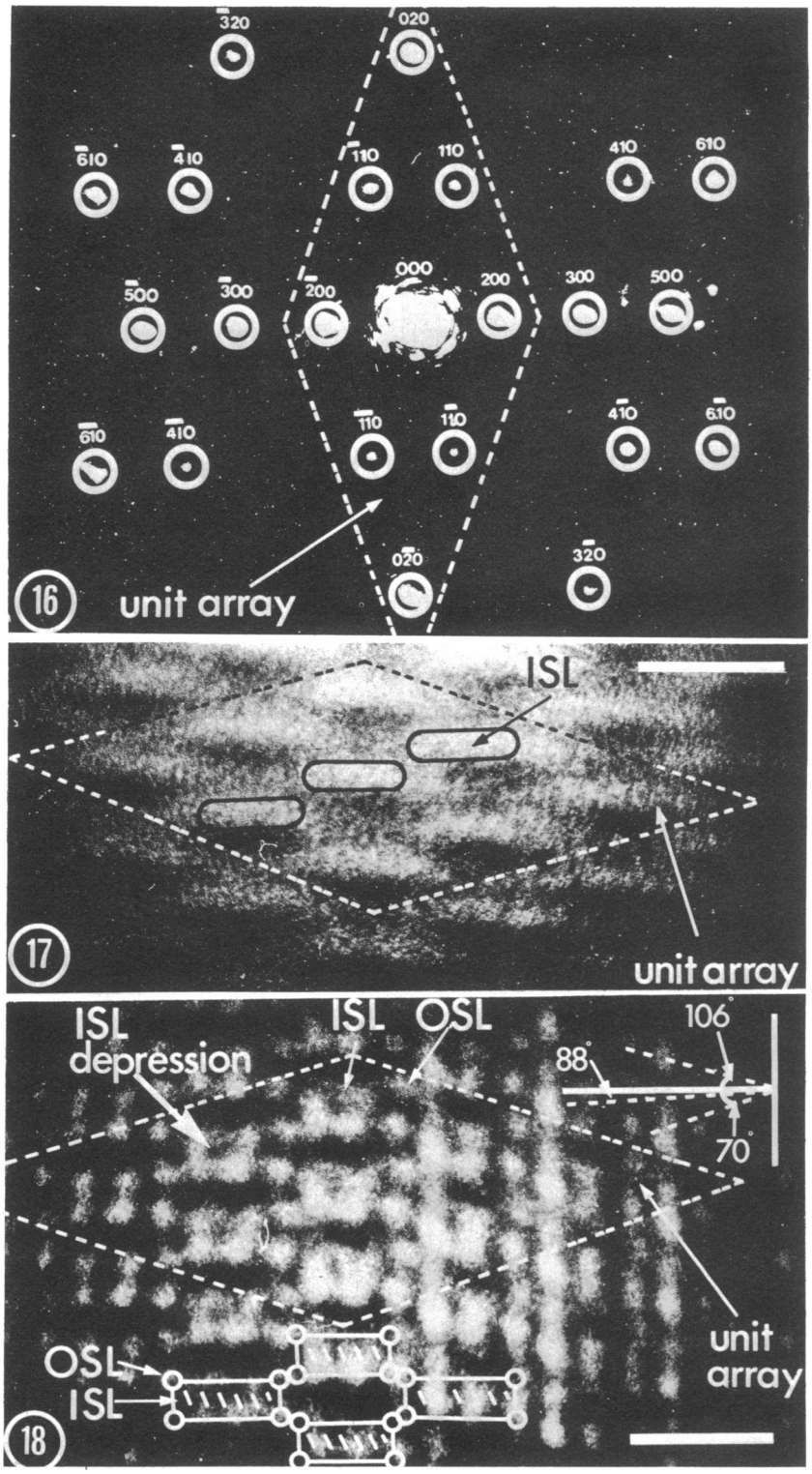

FIG. 16. *Optical transform derived from an ammonium molybdate-stained, intact RS fragment. The indexes responsible for the unit array are circled by the stippled line.*

FIG. 17. *A reconstructed image using only the indexes responsible for the general shape and alignment of the RS (those which are labeled "unit array" in Fig. 18). The unit array of 9 ISL particles is circled by the stippled line. Bar = 10 nm.*

FIG. 18. *A reconstructed image using the total transform (Fig. 16). The ISL and OSL are clearly seen and are aligned at the proper alignment angles. The OSL-ISL complexes have been diagrammatically added to aid interpretation. The unit array is encircled by the stippled line. Bar = 10 nm.*

the base line. These peculiarities confirmed the skewed tetragon revealed by linear integration and also suggested an intimate association between OSL and ISL subunits.

Reconstruction techniques, using masks to allow the passage of selected indexes, have allowed sequential reconstruction of the two RS arrays. The image constructed by the unit array indexes (200, 110, 020, $1\bar{1}0$, $\bar{2}00$, $\bar{1}\bar{1}0$, $0\bar{2}0$, $1\bar{1}0$, and 000) exposed the general shape and packing of the ISL (Fig. 17). Addition of the remaining indexes exposed the OSL and clarified the ISL (Fig. 18). The OSL units could not be individually resolved by reconstruction (lens aberration and focusing difficulty), and it appeared that each OSL globule actually consisted of two OSL units (see diagram, Fig. 18). Total reconstruction of the ISL suggested a complexity hitherto unseen (Fig. 18) and raised the possibility of substructure for each ISL unit (see large arrow, Fig. 18).

Optical diffraction of partially intact fragments (Fig. 5) presented the transform seen in Fig. 19. The existence of spots $\bar{1}10$ and $1\bar{1}0$ suggested that this was not a simple tetragonal packing system. In fact this transform was similar to that given by the intact fragment (Fig. 16), except that those indexes describing the OSL ($6\bar{1}0$, 410, $\bar{3}20$, $\bar{4}10$, $\bar{6}10$, $\bar{6}\bar{1}0$, $\bar{4}\bar{1}0$, $3\bar{2}0$, $4\bar{1}0$, and $6\bar{1}0$) were absent, and four spots (OXO, $\bar{Y}$ZO, O$\bar{X}$O, and Y$\bar{Z}$O) previously undetected were seen. For convenience the position of 110 and $\bar{1}\bar{1}0$ are also indicated in Fig. 19.

Model system. From the previous data on the OSL-ISL complex the model seen in Fig. 20 was drawn. In this model 6- by 3-nm ISL subunits are aligned at 70° and 106° to the longitudinal axis, while spherical 1.5-nm OSL subunits are situated at each of the ISL subunit's corner apexes. No attempt was made to further define the shape of the ISL and OSL subunits other than the rectangular and spherical forms shown, although these were drawn to scale. Due to the observed skew in the ISL alignment, the lateral ISL alignments of 70° and 106° have been incorporated into the model. This necessitated a reciprocal skew of 2° off the perpendicular for every third laterally opposed subunit (Fig. 20).

Figure 21 shows the transform derived from a reduced transparency of the model, the reduction corresponding exactly with the magnification of the OSL-ISL fragment which gave the transform in Fig. 16. The spacings and diffrac-

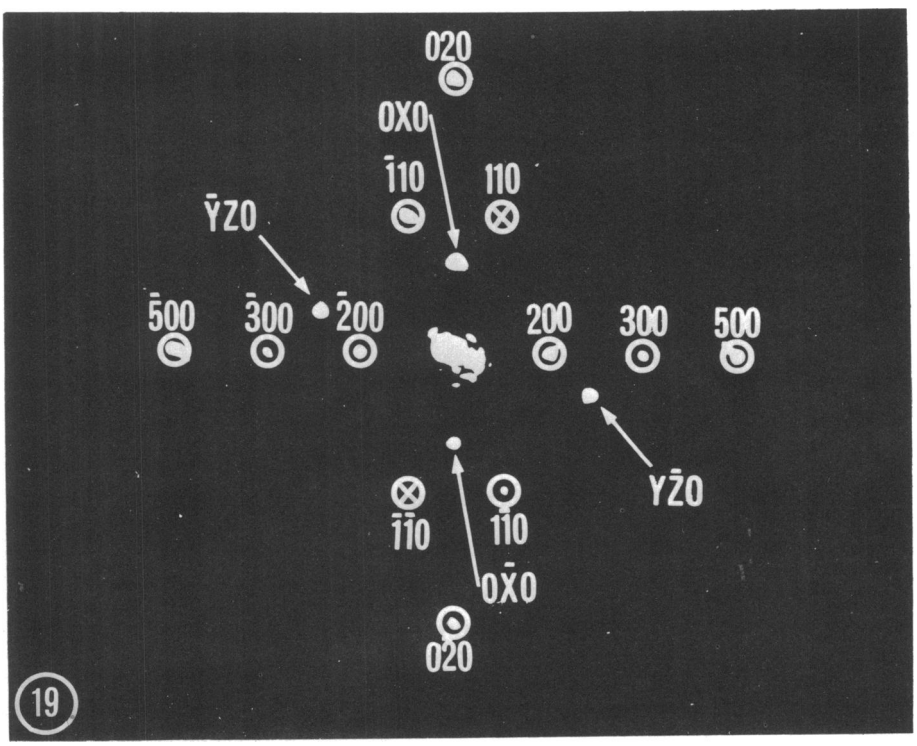

FIG. 19. *Optical transform derived from a partially intact RS fragment (Fig. 5). Indexes 110 and $\bar{1}\bar{1}0$, although not present, have been added to aid interpretation.*

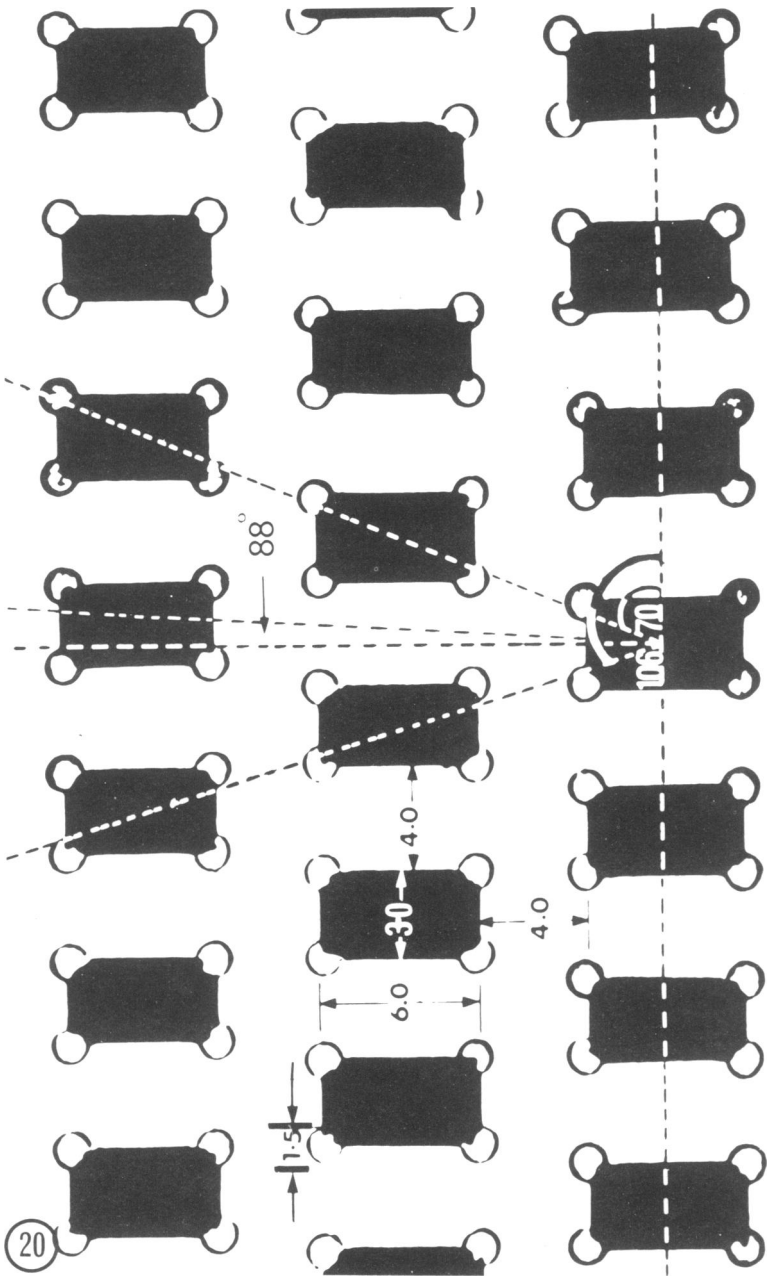

FIG. 20. *Diagrammatical model, drawn to scale, of the surface of the OSL-ISL complex. The alignment angles and dimensions (in nm) have been added. The ISL units have been drawn as rectangular blocks, the OSL units as simple spheres. To aid interpretation the OSL units have not been filled in. The longitudinal (linear) axis runs from the bottom to the top of the page.*

tion angles of the model system corresponded exactly to those given by the intact fragment. Only the spots indexed $\bar{5}20$ and $5\bar{2}0$ (see small arrows, Fig. 21) were unaccounted for and appeared to describe an extremely small spacing aspect of the OSL in our model which was not found in the intact fragment. Changes in subunit size and/or alignment failed to rectify this problem and brought about drastic alteration in the diffraction pattern. Since the OSL

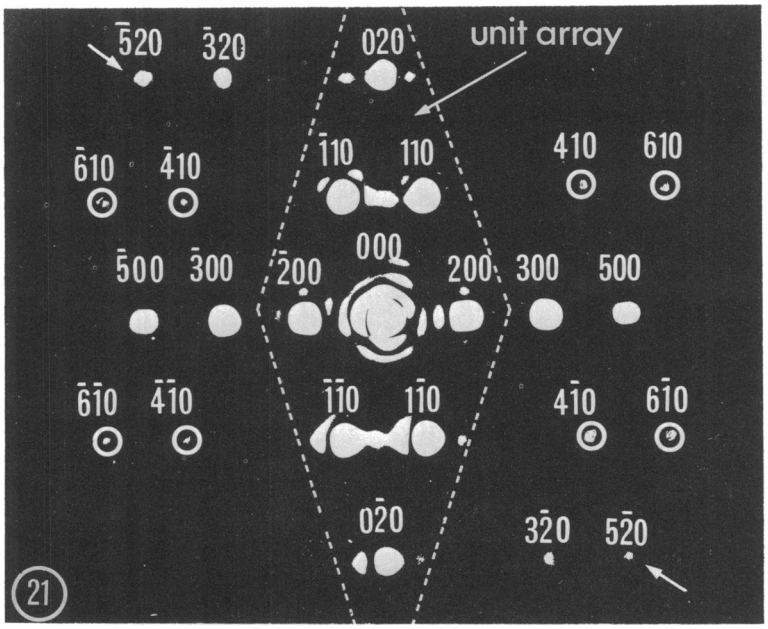

FIG. 21. *Optical transform derived from a photographically reduced image of the model seen in Fig. 20. The correspondence between it and the transform from the intact RS fragment (Fig. 16) is almost exact. The indexes responsible for the unit array are encircled by the stippled line.*

units of our model were hollow (an intentional artifact to separate the OSL and ISL units), these indexes could describe this aspect. Reconstruction of the image using only indexes 110, 020, $\bar{1}10$, $\bar{2}00$, $\bar{1}\bar{1}0$, $0\bar{2}0$, $1\bar{1}0$, 200, and 000 verified that these described the ISL subunits (Fig. 23, "unit array" is indicated), since the unmasked image contained OSL elements (Fig. 22). Additions of indexes 610, 410, $\bar{3}20$, $\bar{4}10$, $\bar{6}10$, $\bar{6}\bar{1}0$, $\bar{4}\bar{1}0$, $3\bar{2}0$, $4\bar{1}0$, and $6\bar{1}0$ which describe the OSL, plus indexes 500, 300, $\bar{3}00$, and $\bar{5}00$ which give the RS its linearity, reconstructed an image (Fig. 24) comparable to the unfiltered image (Fig. 22). Reconstruction did not tell us what dimensional aspects were described by spots $\bar{5}20$ and $5\bar{2}0$; in all other respects this tool proved a powerful means of verifying the validity of our model.

Negatively stained cell margins. Some information was obtainable from the cell edge-stain interface of negatively stained cells, since the margin represented a profile of units as they travelled over the edge. Given an indication of the orientation of the edge relative to the alignment angles of the OSL and ISL subunits we could predict and verify the aspects observed. Because of this, we expected that only those cell-edge stain interfaces which followed along alignment angles would have the OSL-ISL subunits "in phase" and, therefore, easily recognizable. When the longitudinal axis was parallel to the cell edge, the OSL could clearly be seen, but the individual subunits were not resolved (Fig. 2 and 27). The ISL showed a profile depth of about 7 to 8 nm. When the OSL-ISL longitudinal axis was at right angles to the cell edge, the profile showed a scalloped edge formed by the OSL units projecting from the outer corners of the ISL units (Fig. 25). Our model suggested that, in this circumstance, there should be a gradual progression of alternate ISL untis going "in phase" and "out of phase." This was, in fact, hard to confirm. Two OSL-ISL complexes, thought to be in phase, are circled in Fig. 25. A greatly enlarged negative image of one of these complexes (Fig. 26) suggested a Y configuration, the OSL forming the arms and the ISL the base. The ISL unit appeared to have a constricted center region. This profile was quite different than that seen on margins which had OSL-ISL arrays parallel to the cell edge (Fig. 27). In this case, the ISL units appeared rectangular, and the OSL units compacted into a single adjacent layer.

Rotary integration of reassembled OSL-ISL-LPS vesicles. Another source of information concerning the OSL-ISL profile was obtained from the natural reassemblies of the surface structures on an LPS-like component to form tubes or vesicles after RS extraction (unpublished observation). Figure 28 demonstrates a LPS-like vesicle surrounded by reassembled OSL-ISL subunits. Rotary integration of this

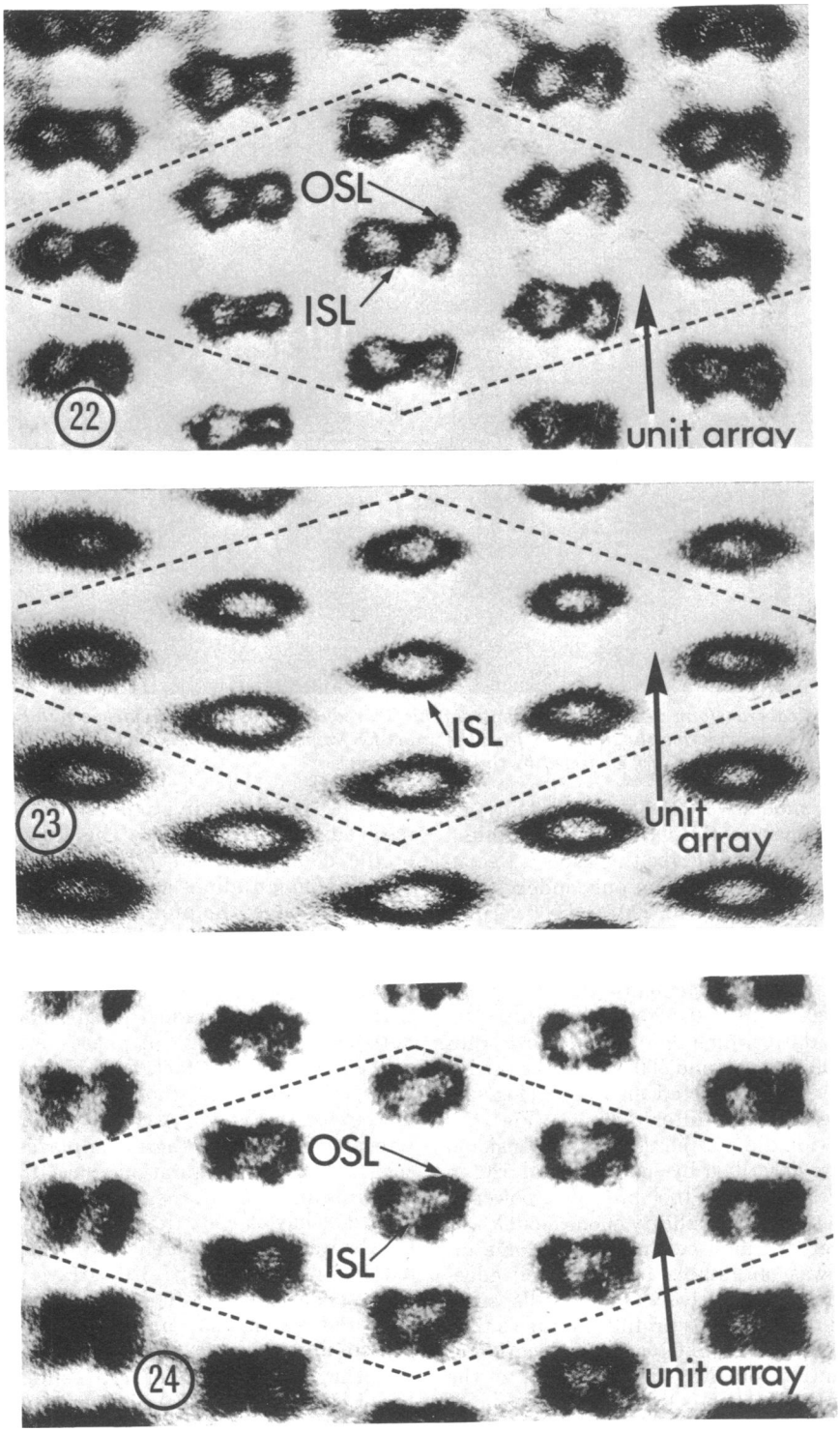

FIG. 22. *Reconstruction of image of the model from the transform of Fig. 21 without mechanical filtration of light. In this and the following reconstructions the OSL-ISL units appear as a negative image to those seen in Fig. 17 and 18, and the stippled line encircles the unit array.*

FIG. 23. *Reconstruction of image using only those indexes responsible for the unit array (those encircled by stippled line in Fig. 21). Only the ISL units may be seen.*

FIG. 24. *Reconstruction of image using the total optical transform of Fig. 21. The ISL unit is a definite rectangular block, and traces of the OSL units can be seen at the ISL corners. These would be more definite if we had filled in the OSL spheres of our model.*

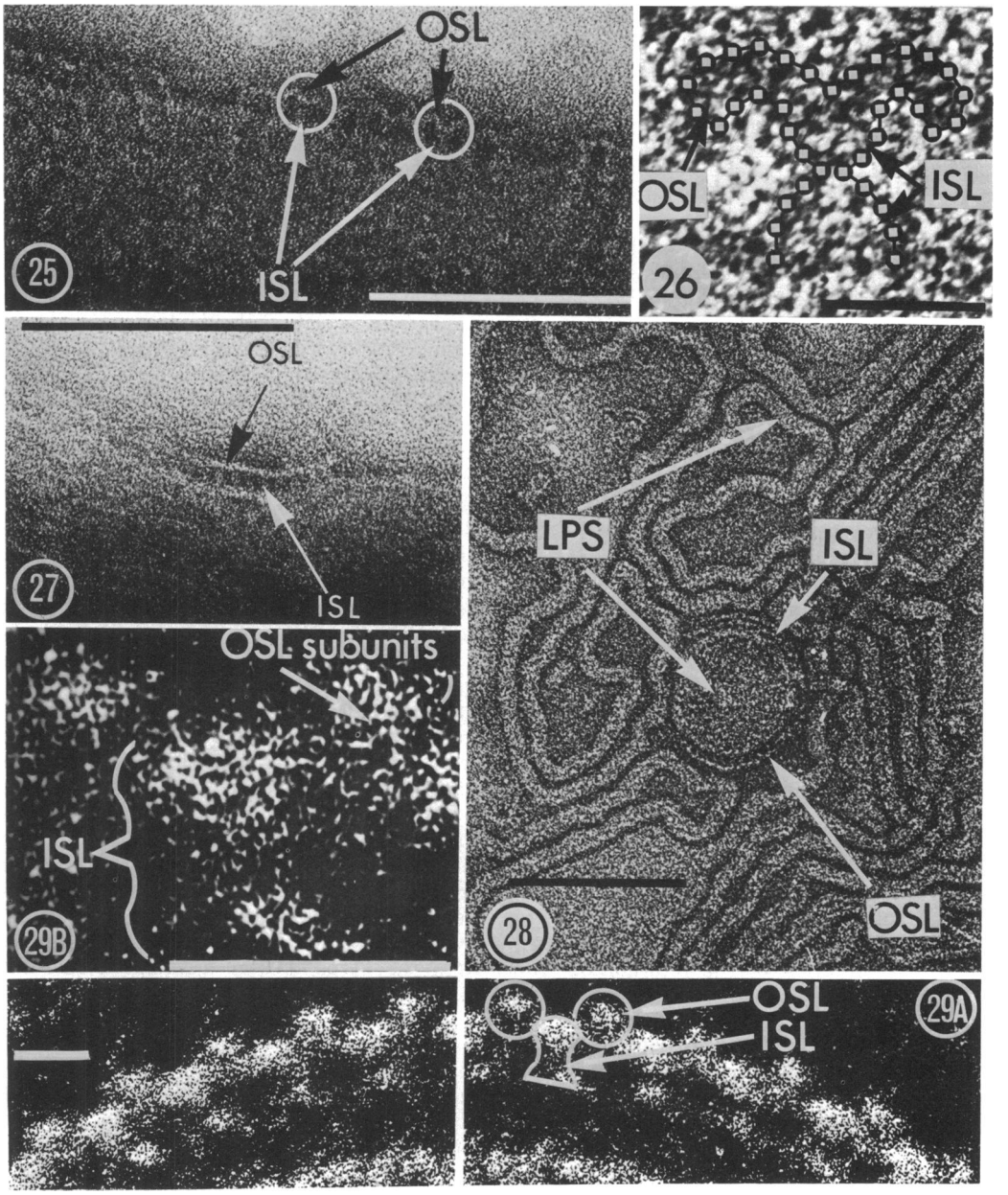

FIG. 25. *Ammonium molybdate-stained cell edge at right angles to the linear array showing the profile of OSL-ISL units. "In phase" OSL-ISL units are circled. Bar = 0.1 μm.*

FIG. 26. *High magnification and negative image of one of the "in phase" OSL-ISL units from Fig. 25. Notice the narrowed waist of the ISL profile. Bar = 10 nm.*

FIG. 27. *Ammonium molybdate-stained cell edge showing the profile of OSL-ISL units running parallel to the longitudinal (linear) axis. Note that the ISL units appear to be simple, rectangular blocks. Bar = 0.1 μm.*

FIG. 28. *Ammonium molybdate-stained, reassembled OSL-ISL-LPS vesicle. The OSL-ISL units can be seen as circumferential particles around the vesicle. Ribbons of "naked" LPS can be seen surrounding the vesicle. Bar = 0.1 μm.*

FIG. 29. *(A) Image formed after rotary integration of the OSL-ISL-LPS vesicle (Fig. 28). The ISL units have a narrowed waist. The OSL globules, although not further resolvable, actually consist of two OSL units. Disk speed = 260 rpm; stroboscopic frequency = ca. 2,600 cycles/min; bar = 10 nm. (B) High magnification of one OSL-ISL unit from (A) showing narrowed ISL waist. Bar = 10 nm.*

micrograph emphasized the OSL-ISL profile (Fig. 29A). Although the individual OSL subunits were not visualized, the profile of the ISL subunit consisted of a broad head and base connected by a thinner neck (Fig. 29A, B) which substantiated that seen in Fig. 26. We suggest that each OSL globule actually consists of two unresolved neighboring OSL subunits, each displaced towards each other and slightly off their respective ISL subunits by the action of the stain, since the diameter measurement of each globule is twice that of the OSL subunit from our model.

DISCUSSION

Many spirilla exhibit close-packed (hexagonal) arrays of macromolecules on the external surface of their cell walls, and *S. serpens* is a prime example (30); some of these have an additional RS layer (e.g., *S. sinuosum*, unpublished observations in this laboratory). Other species show completely different surface patterns, and an example is demonstrated in this paper: *S. putridiconchylium*, a fresh-water spirillum, possesses a novel arrangement of two morphologically distinct surface RS components forming a predominantly linear structure. This complex but highly ordered arrangement lies external and adjacent to the LPS outer membrane. This is the first detailed study of a double RS layer on a *Spirillum* species not involving a hexagonal array.

The existence of the two morphological RS entities (the OSL and ISL) was not confirmed until these units were individually resolved by applying image averaging techniques to micrographs of intact, negatively stained RS fragments. Combination of the information from the optical transforms of partially intact fragments (Fig. 5) and linear integration of intact fragments (Fig. 14, 15) suggested the existence of the ISL below the more obvious OSL. Partially intact fragments released from cells in stationary cultures provided isolated pieces of the ISL (not obtainable by any mechanical means, such as sonication), but they were rare and they appeared to be in various states of disrepair. This may explain the difficulty we experienced in obtaining optical transforms of selected areas of these fragments containing all the index points that described the intact unit array (i.e., in Fig. 19 indexes 110 and $\bar{1}\bar{1}0$ are missing); many showed more obvious deformities in the unit array. The OSL was more friable and was not found by itself.

Optical diffraction provides a precise technique for checking the validity of our interpretation of subunit arrangement; this consists of comparing the optical diffraction pattern of drawn models, reduced to appropriate dimensions, with that of the intact fragment. The transform (Fig. 21) arising from our model (Fig. 20) is remarkably similar and validated most of our assumptions. To our knowledge, this is the first example of such an approach to the interpretation of biological structures.

Information derived from study of folded edges of RS layers suggests that the profile of the ISL unit might differ according to the alignment of the units to the fold. When the RS alignment is parallel to the margin, the ISL unit appears as a rectangular body devoid of other structure (Fig. 27), yet when it is perpendicular to the edge the unit appears to have a narrow waist (Fig. 25, 26). It is possible that this latter image is due to reinforcement from the units immediately preceding and succeeding the marginal ISL unit, but rotary integration of a small OSL-ISL-LPS vesicle, i.e., with circumferential RS, provides a similar waisted profile of the ISL unit (Fig. 29A, B). We must interpret rotary integration with caution (12), but our calculations of expected numbers of circumferential RS units and the images formed by slight stroboscopic frequency changes suggest that the images of Fig. 29A and B are not totally artifactual. Some thin sections of RS also demonstrate a similar aspect of the ISL (Fig. 11), and here the orientation of the section is critical. In all cases, whether sectioned or negatively stained, the OSL units appear to occur at the external corners of the ISL subunits. If our interpretation of this data is correct, it would seem that the profile of the ISL unit depends upon the direction of view; if viewed parallel to the cell axis, it would have a solid rectangular shape, whereas from the perpendicular it would have a narrowed waist.

As with *S. serpens*, the RS of *S. putridiconchylium* requires Ca^{2+} for stability, indicating that non-covalent bonding is a factor in maintaining integrity and wall retention (6, 7). The ability of the RS to slough off the wall in late logarithmic and stationary cultures may indicate depletion of stabilizing Ca^{2+}. Retention of the RS on embedded and sectioned cells was increased by the addition of ruthenium red, although neither alcian blue (35) nor silver methenamine (10) demonstrated polysaccharide in the RS. It seems possible that ruthenium red acts as a polyvalent cation to stabilize the RS. Its size (ca. 1.1 nm [24]) would allow it to fit between the ISL units, and its charge (6+) could form strong salt bridges within the RS, thus increasing resistance to the disruptive influences of the embedding technique.

The stabilizing influence of Ca^{2+} suggests that the RS units are anionic and they are

probably proteinaceous (T. Beveridge and R. G. E. Murray, unpublished observations on fractions). The susceptibility of the RS to pH $\leqslant$ 4.6 indicates that under these acidic conditions the RS anion has been either saturated with H^+ or amphoterically altered, thereby resulting in a disruption of the macromolecular arrangement. The RS was also damaged by organic solvents as shown by the loss of this structure when cells are dehydrated with either acetone or ethanol before embedding in Vestopal W or Epon 812 (Fig. 8). It is not clear what component(s) of the RS or the substrate outer membrane might be extracted or denatured by these solvents. This susceptibility was not exhibited by *S. serpens* (5, 6) but has been demonstrated in parallel experiments in our laboratory on *S. metamorphum* and, to a lesser degree, on the *Spirillum* "Ordal."

It is of interest to note that McElroy and Krieg (26) found nonreciprocal cross-agglutination using antisera derived from the thermolabile antigens of *S. putridiconchylium* (ATCC 15278) and the whole cells of two strains of *S. serpens*, one of which was a VH strain. Of the two VH strains in our laboratory, one (VHA) possesses a hexagonal RS and the other (VHL) is a "naked" mutant strain. The RS layers of both VHA and *S. putridiconchylium* are thermolabile (7; T. Beveridge and R. G. E. Murray, unpublished data). Since we have just demonstrated that the superficial wall structure of *S. putridiconchylium* is morphologically different than that of *S. serpens*, it appears remarkable that such a relationship could exist, unless, independent of the RS components, a common thermolabile antigen (i.e., flagella or outer membrane component) accounts for this serological cross-reaction.

ACKNOWLEDGMENTS

We are grateful to M. Hall for expert technical assistance, J. Marak for electron microscopical advice, and G. Saunders for photographic suggestions. We also appreciate the interest of I. D. J. Burdett in this project.

The generous support of the Medical Research Council of Canada is gratefully acknowledged.

LITERATURE CITED

1. Adelberg, E A., M. Mandel, and G. C. C. Chen. 1965. Optimal conditions for mutagenesis by N-methyl-N'-nitro-N-nitrosoguanidine in *E. coli* K12. Biochem. Biophys. Res. Commun. **18**:788-795.
2. Braun, V., and V. Bosch. 1972. Sequence of the murein-lipoprotein and the attachment site of the lipid. Eur. J. Biochem. **28**:51-69.
3. Braun, V., H. Gnirke, U. Henning, and K. Rehn. 1973. Model for the structure of the shape-maintaining layer of the *Escherichia coli* cell envelope. J. Bacteriol. **114**:1264-1270.
4. Braun, V., and U. Sieglin. 1970. The covalent murein-lipoprotein structure of *Escherichia coli* cell wall. The attachment site of the lipoprotein on the murein. Eur. J. Biochem. **13**:336-346.
5. Buckmire, F. L. A. 1970. The physical structure of the cell wall as a differential character. Int. J. Syst. Bacteriol. **20**:345-360.
6. Buckmire, F. L. A., and R. G. E. Murray. 1970. Studies on the cell wall of *Spirillum serpens*. I. Isolation and partial purification of the outermost cell wall layer. Can. J. Microbiol. **16**:1011-1022.
7. Buckmire, F. L. A., and R. G. E. Murray. 1973. Studies on the cell wall of *Spirillum serpens*. II. Chemical characterization of the outer structured layer. Can. J. Microbiol. **19**:59-66.
8. Chapman, J. A., R. G. E. Murray, and M. R. T. Salton. 1963. The surface anatomy of *Lampropedia hyalina*. Proc. Roy. Soc. B **158**:498-513.
9. Cox, R. W., and R. W. Horne. 1968. Accurate calibration of the A. E. I. E. M. 6B/2 electron microscope using catalase crystals, p. 579-580. Fourth European Regional Conference on Electron Microscopy, Rome. Tipographia Poliglotta Vaticana.
10. de Martino, C., and L. Zamboni. 1967. Silver methenamine stain for electron microscopy. J. Ultrastruct. Res. **19**:273-282.
11. Ellar, D. J., and D. G. Lundgren. 1967. Ordered substructure in the cell wall of *Bacillus cereus*. J. Bacteriol. **94**:1778-1780.
12. Friedman, M. H. 1970. A reevaluation of the Markham rotation technique using model systems. J. Ultrastruct. Res. **32**:226-236.
13. Glauert, A. M., and M. J. Thornley. 1969. The topography of the bacterial cell wall. Annu. Rev. Microbiol. **23**:159-198.
14. Harris, J. R., and P. Agutter. 1970. A negative staining study of human erythrocyte ghosts and rat liver nuclear membranes. J. Ultrastruct. Res. **33**:219-232.
15. Hayat, M. A. 1970. Principles and techniques of electron microscopy: biological applications, vol. 1. Van Nostrand Reinhold Co., New York.
16. Holt, S. C., and E. R. Leadbetter. 1969. Comparative ultrastructure of selected aerobic spore-forming bacteria: a freeze-etching study. Bacteriol. Rev. **33**:346-378.
17. Horne, R. W., and R. Markham. 1972. Application of optical diffraction and image reconstruction techniques to electron micrographs. *In* A. M. Glauert (ed.), Practical methods in electron microscopy, vol 1. American Elsevier Publishing Co., Inc., New York.
18. Howard, L., and D. J. Tipper. 1973. A polypeptide bacteriophage receptor: modified cell wall protein subunits in bacteriophage-resistant mutants of *Bacillus sphaericus* strains P-1. J. Bacteriol. **113**:1491-1504.
19. Klug, A., and J. E. Berger. 1964. An optical method for the analysis of periodicities in electron micrographs and some observations in the mechanism of negative staining. J. Mol. Biol. **10**:565-568.
20. Klug, A., and D. J. DeRosier. 1966. Optical filtering of electron micrographs: reconstruction of onesided images. Nature (London) **212**:29-32.
21. Leadbetter, E. R., and S. C. Holt. 1968. The fine structure of *Bacillus fastidiosus*. J. Gen. Microbiol. **52**:299-307.
22. Leduc, E. H., and S. J. Holt. 1965. Hydroxypropyl methacrylate, a new water-miscible embedding medium for electron microscopy. J. Cell Biol. **26**:137-155.
23. Luft, J. H. 1961. Improvements in epoxy resin embedding methods. J. Biophys. Biochem. Cytol. **9**:409-414.
24. Luft, J. H. 1971. Ruthenium red and violet. I. Chemistry, purification and methods for use in electron microscopy and mechanism of action. Anat. Rec. **171**:347-368.
25. Maier, S., and R. G. E. Murray. 1965. The fine structure of *Thioploca ingrica* and a comparison to *Beggiatoa*.

Can. J. Microbiol. **11**:645-655.
26. McElroy, L. J., and N. R. Krieg. 1972. A serological method for the identification of *spirilla*. Can. J. Microbiol. **18**:57-64.
27. Markham, R., S. Frey, and G. J. Hills. 1963. Methods for the enhancement of image detail and concentration of structure in electron microscopy. Virology **20**:88-102.
28. Markham, R., J. H. Hitchburn, G. J. Hills, and S. Frey. 1964. The anatomy of the tobacco mosaic virus. Virology **22**:342-359.
29. Mellema, J. E., E. F. J. van Bruggen, and M. Gruber. 1968. An assessment of negative staining in the electron microscopy of low molecular weight proteins. J. Mol. Biol. **31**:75-82.
30. Murray, R. G. E. 1963. On the cell wall structure of *Spirillum serpens*. Can. J. Microbiol. **9**:381-391.
31. Nermut, M. V., and R. G. E. Murray. 1967. Ultrastructure of *Bacillus polymyxa*. J. Bacteriol. **93**:1949-1965.
32. Reyn, A., A. Birch-Andersen, and R. G. E. Murray. 1971. The fine structure of *Cardiobacterium hominis*. Acta Pathol. Microbiol. Scand. Sect. B **79**:51-60.
33. Reynolds, E. S. 1963. The use of lead citrate at high pH as an electron-opaque stain in electron microscopy. J. Cell. Biol. **17**:208-212.
34. Ryter, A., and E. Kellenberger. 1958. L'inclusion au polyester pour l'ultramicrotomie. J. Ultrastruct. Res. **2**:200-214.
35. Scott, J. E., G. Quintarelli, and M. C. Dellovo. 1964. The chemical and histochemical properties of alcian blue. I. The mechanism of alcian staining. Histochemie **4**:73-85.
36. Sleytr, U. B., and M. J. Thornley. 1973. Freeze-etching of the cell envelope of an *Acinetobacter* species which carries a regular array of surface subunits. J. Bacteriol. **116**:1383-1397.
37. Taylor, C. A., and H. Lipson. 1964. Optical transforms. G. Bell and Sons Ltd., London.
38. Thorne, K. J. I., M. J. Thornley, and A. M. Glauert. 1973. Chemical analysis of the outer membrane and other layers of the cell envelope of *Acinetobacter* sp. J. Bacteriol. **116**:410-417.
39. Thornley, M. J., and A. M. Glauert. 1968. Fine structure and radiation resistance in *Acinetobacter*: studies on a resistant strain. J. Cell Sci. **3**:273-294.
40. Thornley, M. J., A. M. Glauert, and U. B. Sleytr. 1973. Isolation of outer membranes with an ordered array of surface subunits from *Acinetobacter*. J. Bacteriol. **144**:1294-1308.
41. Watson, S. W., and C. C. Remsen. 1970. Cell envelope of *Nitrosocystis oceanus*. J. Ultrastruct. Res. **33**:148-160.